Etched-cavity GaSb laser diodes on a MOVPE GaSb-on-Si template

Laura Monge-Bartolomé, Tiphaine Cerba, Daniel A Díaz-Thomas, Michaël Bahriz, Marta Calvo, Guilhem Boissier, Thierry Baron, Jean-Baptiste Rodriguez, Laurent Cerutti, Eric Tournié

Research Article | Vol. 28, No. 14 / 6 July 2020 / Optics Express 20785

Optics EXPRESS

Etched-cavity GaSb laser diodes on a MOVPE GaSb-on-Si template

LAURA MONGE-BARTOLOME,[1] TIPHAINE CERBA,[2,3] DANIEL A. DÍAZ-THOMAS,[1] MICHAËL BAHRIZ,[1] MARTA RIO CALVO,[1] GUILHEM BOISSIER,[1] THIERRY BARON,[2] JEAN-BAPTISTE RODRIGUEZ,[1] LAURENT CERUTTI,[1] AND ERIC TOURNIÉ[1,4,*]

[1]*IES, University of Montpellier, CNRS, F-34000 Montpellier, France*
[2]*Univ. Grenoble Alpes, CNRS, CEA-LETI, MINATEC, LTM, F-38054 Grenoble, France*
[3]*Currently with III-V Lab, 1 rue Augustin Fresnel, F-97167 Palaiseau, France*
[4]*On leave at Institute for Nano Quantum Information Electronics, The University of Tokyo, Japan*
[*]*eric.tournie@umontpellier.fr*

Abstract: We report on 2.3-µm etched-cavity GaSb-based laser diodes (LDs) epitaxially integrated on on-axis (001)Si and benchmarked against their cleaved facet counterparts. The LDs were grown in two steps. First, a GaSb-on-Si template was grown by metal-organic vapor phase epitaxy (MOVPE) before the growth of the LD heterostructure by molecular-beam epitaxy. Different etched-facet geometries operate in continuous wave well above room temperature, and their performance are similar to those of cleaved-cavity LDs. These results show that etching mirrors is a viable route to form laser cavities in the GaSb technology and that MOVPE GaSb-on-Si templates are a suitable platform for optoelectronic devices overgrowth.

1. Introduction

The short-wave (1.6–3 µm range) part of the mid-infrared (mid-IR) wavelength range has attracted great interest because many molecules such as hydrocarbons (including methane and ethane), hydrochloric acid, ethanol, ammonia, exhibit strong photon absorption peaks within these wavelengths [1]. It is thus well suited for implementing a variety of high societal-impact photonic sensors or devices. High efficiency GaSb-based laser diodes (LDs) are now available in this range [2,3] and their heterogeneous integration with Silicon-based platforms is under active consideration with the objective to develop compact, cost-effective, smart sensing systems based on Si photonic integrated circuits (PICs) [4].

Another, longer-term, option is the epitaxial integration of GaSb LDs directly on Si since this approach should outperform heterogeneous integration, provided on-axis, CMOS-compatible, (001)-oriented Si substrates can be used [5]. A sensing strategy in that case is based on coplanar lasers and detectors, as demonstrated on InP platforms [6,7]. This, however, requires laser cavities to be fabricated directly at the wafer scale through facet etching, a technology which is not yet available with the GaSb materials system.

Only recently were high-performance GaSb mid-IR LDs epitaxially integrated on on-axis (001)Si demonstrated [8]. These LDs were grown by molecular-beam epitaxy (MBE), the only technique to date able to grow high-performance GaSb-based light sources [2,3]. Still, all these lasers were discrete devices with Fabry-Pérot cavities formed by cleaving the III-V-on-Si epitaxial wafer, a technique obviously incompatible with any PIC strategy.

On another hand, GaSb layers grown by metal-organic vapor phase epitaxy (MOVPE) on 300-mm on-axis (001)Si substrates have also recently been reported [9]. Provided high-performance light sources can be grown atop, on-wafer laser-cavity definition and large-dimension GaSb-on-Si wafers could offer a cost-effective solution to implement large-scale integration of mid-IR photonics sensors.

#397164 https://doi.org/10.1364/OE.397164
Journal © 2020 Received 7 May 2020; revised 8 Jun 2020; accepted 11 Jun 2020; published 29 Jun 2020

Optics EXPRESS

In this article, we report on etched-facet GaSb-based LDs grown on a GaSb-on-Si template previously grown by MOVPE and emitting at 2.3 µm.

2. Epitaxial growth

The epitaxial growth flow is schematically depicted in Fig. 1. First a 500-nm thick, non-intentionally doped, *p*-type, GaSb buffer layer was grown by MOVPE on a 300-mm diameter (001) Si substrate as described in Sec. 2.1. Subsequently, 50-mm diameter slices were diced into this master wafer to produce GaSb-on-Si templates which were transferred to another laboratory for the MBE growth of LDs (Sec. 2.2).

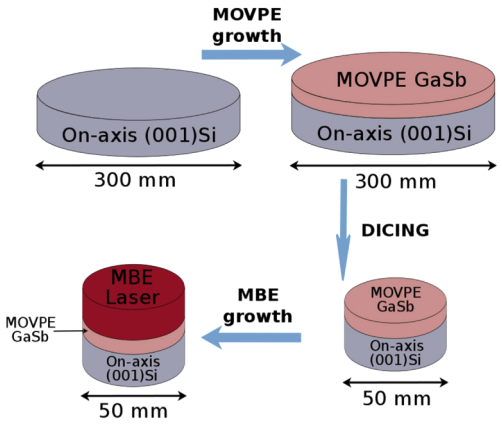

Fig. 1. Epitaxial growth-flow.

2.1. MOVPE of the GaSb-on-Si template

The GaSb buffer epitaxy was carried out on standard 300 mm (001) Si wafers used in the microelectronics industry, presenting an offcut angle of 0.11° in the [1 1 0] direction and a resistivity in the 5–10 Ω.cm range. We used an Applied Materials cluster tool equipped with surface preparation and epitaxy modules. Before the growth, any contamination and presence of native oxide were eliminated by using a SiCoNi cleaning process [10]. The SiCoNi chamber relied on a deported NH_3/NF_3 plasma which reacted with the native silicon oxide to form a thin $(NH_4F)_2SiF_6$ solid layer at the surface. This layer was then removed by thermal treatment, leaving the Si surface hydrogen-passivated. The wafers were then transferred under vacuum in the epitaxy chamber, which is an MOVPE reactor using tri-ethyl-antimony (TESb) as group-V precursor and trimethylgallium (TMGa) as group III-precursor.

To promote the surface reconstruction and the formation of Si double steps, a high temperature annealing under ultra-pure hydrogen at high pressure was performed [11]. Particular attention was paid to avoid that anti-phase boundaries (APBs), structural defects created at the interface between the non-polar Si substrate and the polar III-V semiconductor epitaxial material [12], propagate through the GaSb buffer layer. The growth proceeded via a two-step process with a low-temperature nucleation layer, in the 350–450°C range, and a high-temperature layer grown at around 600°C, with a V/III ratio around 1 [9]. After annealing, any residual APBs due to local imperfections of the double-step arrangement at the (001) Si surface were annihilated after a thickness of about 200 nm [9,11] The threading-dislocation density in such template is estimated around 10^9 cm^{-2} [9] whereas the rms roughness measured from 5×5 μm^2 atomic-force microscopy images is typically around 0.5 nm [9].

Optics EXPRESS

After MOVPE growth, the surface of the GaSb-on-Si epitaxial material was protected with a resist before the wafer was diced into 50-mm slices. Each 300-mm wafer gives at least sixteen 50-mm or four 100-mm GaSb-on-Si templates.

2.2. MBE of the laser heterostructure

Prior to being loaded into the MBE reactor, the 50-mm GaSb-on-Si MOVPE template was thoroughly cleaned with organic solvents before being treated with an oxygen plasma to remove any residual resist contamination. The template was then handled in the same way as a regular, epi-ready GaSb substrate [13] and the laser structure was similar to previous ones grown on Si [8,14,15] for the sake of comparison. The wafer was heated up to around 560°C under Sb_2 flux for oxide removal. Then its temperature was decreased down to 500°C for the epitaxy of a 500-nm thick, *n*-doped (N_D-N_A ~1 x10^{18} cm^{-3}) GaSb buffer layer. The total thickness of the GaSb layer (MOVPE + MBE layers) underneath the laser structure was thus 1 µm. Next, we grew a laser structure similar to the one previously described [8]. First, a 500-nm thick, *n*-type, $InAs_{0.92}Sb_{0.08}$ layer was grown at 450°C. This layer, which is lattice-matched to GaSb, served as an etching marker for the subsequent LD processing. This layer was also used to take the back electrical-contact (Fig. 2(a)). This avoids driving the current through the defective III-V/Si interface which results in high turn-on voltage and series resistance. [14] Subsequently, an additional 1-µm thick, *n*-type, GaSb layer was grown right below the LD heterostructure to avoid overlapping of the optical mode with the highly-doped, narrow gap, InAsSb layer. The active zone was made of two $Ga_{0.67}In_{0.33}As_{0.12}Sb_{0.88}$ quantum wells (QWs) confined by $Al_{0.25}Ga_{0.75}As_{0.02}Sb_{0.98}$ barrier layers. This ensemble, designed to emit near 2.3 µm [2,3], was embedded in an $Al_{0.25}Ga_{0.75}As_{0.02}Sb_{0.98}$ waveguide, itself clad by $Al_{0.9}Ga_{0.1}As_{0.07}Sb_{0.93}$ layers. Graded $Al_xGa_{1-x}As_ySb_{1-y}$ layers have been inserted underneath/above the bottom/top cladding layers to smooth the band profile between GaSb and $Al_{0.9}Ga_{0.1}As_{0.07}Sb_{0.93}$ layers. All layers below the waveguide have been doped *n*-type with N_D-N_A ~1 x10^{18} cm^{-3}. The top cladding layer was *p*-type doped with N_A-N_D ~1 x10^{18} cm^{-3} whereas the *p*-type doping level was progressively increased in the last 200-nm to reach N_A-N_D ~1 x10^{19} cm^{-3} in the GaSb top contact layer. All AlGaAsSb alloys were lattice-matched to GaSb while the $Ga_{0.67}In_{0.33}As_{0.12}Sb_{0.88}$ QWs were

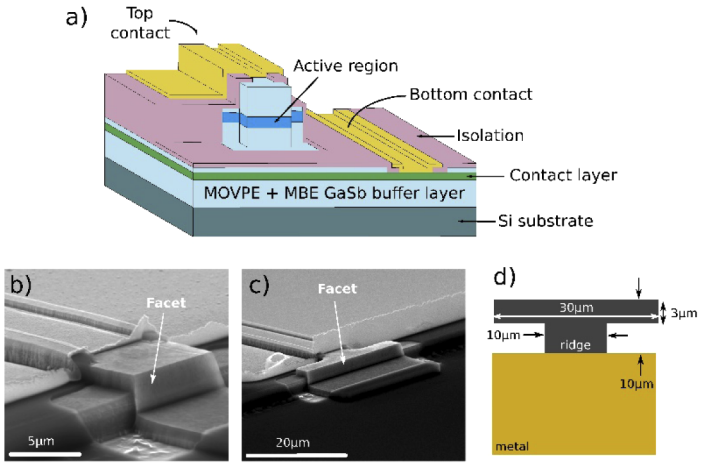

Fig. 2. (a) Scheme of a rectangularly etched-facet laser diode, (b) scanning electron microscopy image of a rectangularly-etched laser-diode facet, (c) scanning electron micrograph of a T-shape etched facet, d) top-down view schematic of the T-shape etched facet (not to scale).

Optics EXPRESS

mismatched by 1.5%. Full relaxation of the LD heterostructure with respect to the Si substrate was confirmed by X-ray diffraction. No dislocation filtering layer was inserted in the structure. Atomic-force microscopy images revealed a threading-defect density in the low 10^8 cm^{-2} range and a rms roughness as low as 1.9 nm. The final epitaxial sample was free of any crack resulting from thermal-expansion-coefficient mismatch.

3. Laser diode processing

In order to characterize the laser-material quality, we fabricated a batch of cleaved-cavity broad area LDs using a standard process which has been previously described in detail [15].

Next, we fabricated both cleaved- and etched-cavity ridge LDs using standard UV photolithography and inductively-coupled plasma reactive-ion etching (ICP-RIE) to define the ridges and – when appropriate (see below) – the cavity mirrors. The AZ1518 photoresist was used as etching mask for the definition of all patterns, including the facets. For the mirror facet definition, we used a (4/2/6.5 sccm) BCl_3/Cl_2/Ar gas mixture, an ICP power of 300 W and a RF power of 60 W, resulting in an etching rate of 370 nm/min. Note that to define the ridge, care was taken to stop the etching into the top-cladding layer, to avoid etching through the active zone (Fig. 2(a)). Vacuum contact between the mask and the sample was used during the light-exposure to obtain vertical flanks and hard-bake was carried out for smoothing the sidewalls. Electrical insulation and protection were obtained with around 350-nm Si_3N_4 deposited by plasma-enhanced chemical vapor deposition (PECVD). Ti-Au was used as contact metal for both *p*- and *n*-type electrodes. Figure 2(b) shows a scanning electron microscopy image of an etched facet at the end of the process. Note that metal deposition was stopped about 10 µm away from the facets to avoid their contamination. No coating was applied to any of the LD facets. Ten-µm wide ridge LDs were fabricated. Their cavity lengths were defined by the lithography mask and ranged from 1 to 2.5 mm. Laser bars were separated by cleaving the wafer approximately 100 µm away from the etched facets (Fig. 2(a)). The bar lengths were measured after cleavage to precisely know the cavity length of the cleaved-facet LDs. Each laser bar thus supported several cleaved- and etched-facet LDs which were tested under pulsed and cw operation at various temperatures. This allowed direct and meaningful comparison between cleaved- and etched- facet LDs. Two types of etched facets, rectangular shape and T-shape, were designed and fabricated (Fig. 2). The rectangular design (Fig. 2(b)) directly mimics a cleaved Fabry-Pérot cavity. However, it exhibits sharp angles which may pose problem during lithography steps. This could result in round corners and/or to defects, both of them inducing mirror losses. T-shape facets (Fig. 2(c)) in contrast allow pushing the corners away from the mirror (Fig. 2(d)) and getting rid of any such a problem.

4. Laser diode characteristics

The broad-area LDs were measured under pulsed operation at room-temperature whereas ridge LDs were studied in cw mode at various temperatures. Their output power was measured by a calibrated power-meter while their emitted spectra were recorded through a grating spectrometer coupled to a cooled InSb photodetector.

4.1. Emission wavelength

We first display in Fig. 3 the laser spectra taken at room-temperature under cw operation from a cleaved cavity and an etched-facet LDs. For both devices the emission is close to 2.3 µm. This confirms that the epitaxial structure was grown according to the design.

4.2. Threshold current density

To get accurate values of threshold current densities, light-current (L – I) measurements were performed on broad-area LDs under pulsed operation. This technique allows to know both the

Optics EXPRESS

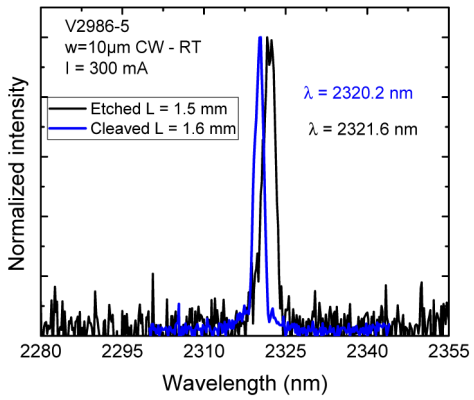

Fig. 3. Spectra taken at room temperature in cw mode from a cleaved-cavity LD and an etched-facet LD.

actual current-injection area and actual device temperature. Figure 4 shows such curves taken at room-temperature from representative broad-area cleaved-cavity LDs with 100 µm ridge width and 1 mm or 1.5 mm cavity length.

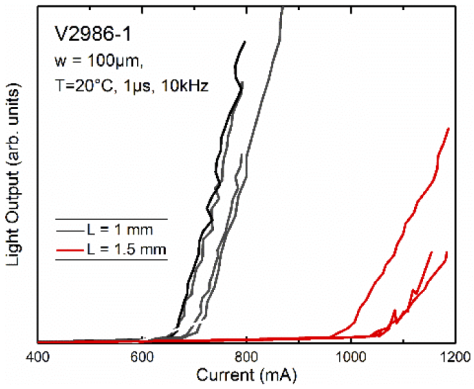

Fig. 4. L – I curves taken at room temperature under pulsed operation from representative cleaved-cavity broad-area LDs with 0.1×1 or $0.1 \times 1.5\ mm^2$ cavities.

The threshold-current densities are around 650–700 $A.cm^{-2}$, identical for all cavity length. This value is significantly lower than that measured (900–1000 $A.cm^{-2}$) with similar LDs grown in an all-MBE process on offcut Si substrates [14] and approaches the value (400–500 $A.cm^{-2}$) obtained on all-MBE on-axis LDs [8].

4.3. Etched vs. cleaved laser diode cavities

Next, we characterized in detail etched-facet ridge LDs and compared them to their cleaved-cavity counterpart. The ridge width was 10 µm for all LDs studied here.

We display in Fig. 5 the L – I – V curves taken at room-temperature under cw operation from series of cleaved- (Fig. 5(a)) and rectangularly etched- (Fig. 5(b)) facet LDs with different cavity lengths. The T-shape etched-facet LDs, not shown here, gave very similar results (see also Fig. 6). This figure shows that both cleaved- and etched- facet LDs behave in similar ways. The turn-on voltage is around 1 V and the series resistances are around 3 to 6 Ω, similar to values for GaSb-based LDs [2,3]. The threshold currents are in the 150–400 mA range for both types of

Optics EXPRESS

facets. At first sight however, the output power and external differential quantum efficiency of the etched-facet LDs seem lower than that of cleaved-cavity LDs. However, this is mainly due to measurement issues. In fact, the etched-cavities being shorter than the laser bars (Fig. 2(a)) and the laser emission being highly divergent in the vertical direction, only part of the emitted light is collected by the photodetector. Imaging the far-field emission of a LD with an IR camera revealed that the photodetector collected around half of the emitted light. This indicates that the emitted power is similar for both types of LDs. Still, no reliable information other than the threshold current can be extracted from the L – I curves taken from the etched-facet LDs.

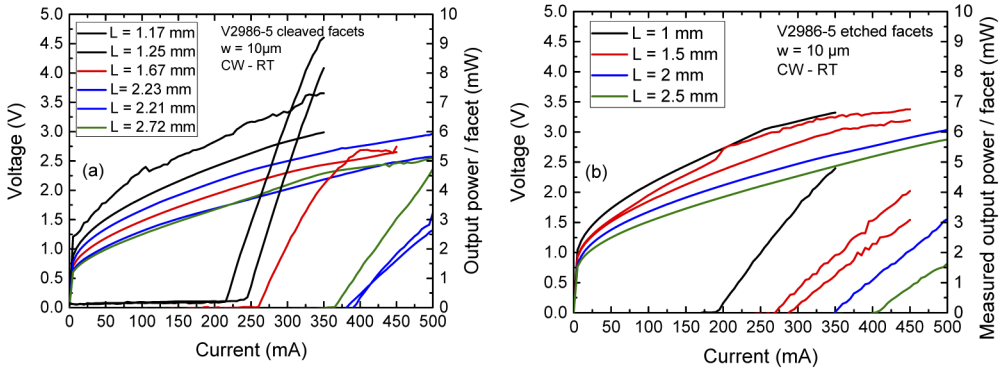

Fig. 5. L-I-V curves taken at room temperature under cw operation for (a) cleaved- and (b) rectangularly etched- facet LDs with a 10-µm ridge width and various cavity length.

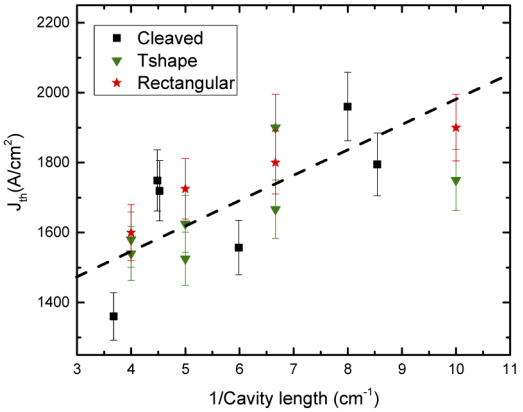

Fig. 6. Comparison of the threshold current density for the three types of laser diodes under investigation (cleaved- rectangularly etched- and T-shape etched- facets), and various cavity length.

We plotted in Fig. 6 the evolution with the inverse of the cavity-length of the threshold current density taken in cw mode at room-temperature for all types of ridge LDs, *i.e.* cleaved-, rectangularly etched- and T-shape etched- facets. All etched-facets LDs exhibit similar threshold current densities whatever their shape. Although some variability can be observed on this figure, we could not relate it to any macroscopic properties (facet image, I-V curves, etc.) of the LDs. Microcospic analysis will be needed to clarify its origin. The interesting point here is that for a given cavity length, all LDs have similar threshold current densities and, consequently, the variations of the threshold current-densities with the cavity length are also similar. Since the

Optics EXPRESS

slope of the J_{th} (1/L) curve is proportional to the power reflectivity of the facets [16,17], Fig. 6 indicates that – within the error bars – etched facets have a power reflectivity similar to that of cleaved facets, a conclusion already drawn from InP [16] and GaAs [17] LDs with etched-mirror cavities.

In addition, the LDs have been studied in cw mode at different temperatures between 20 and 70°C (limited by our experimental setup). Again, all LDs behaved in similar ways. As an example, we show in Fig. 7 the L – I – V curves taken from a 10 µm x 1 mm LD with rectangularly etched facets. Lasing was readily achieved in the whole temperature range. Note that, again, the measured output power is lower than the actual power emitted by the laser, due to the measurement configuration, and one cannot extract the physical parameters of the LDs. Still, Fig. 7 shows that these LDs emit several mW in the whole temperature range, a power high enough to perform sensitive and reliable gas sensing. The inset in Fig. 7 shows the semi-logarithmic plot evolution of the threshold current with the temperature. This translates in a characteristic temperature $T_0 = 85$ K, a value comparable to values generally measured on GaSb LDs grown on their native substrates [2,3].

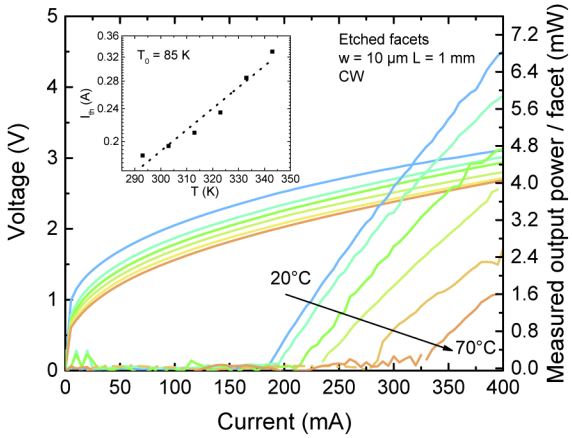

Fig. 7. L – I – V curves taken between 20 °C and 70 °C in cw mode from an etched-facet LD. The inset shows the semi-logarithmic plot of the threshold current as a function of the temperature.

5. Discussion

Our results show that etched-cavity GaSb LDs grown on Si behave very similarly to their cleaved counterparts. The high threading-defect density arising from the large lattice mismatch between GaSb and the Si substrate thus does not preclude the formation of efficient etched-facets. Interestingly, the rectangular and T-shape facets exhibit similar performances which should simplify future processing developments. To the best of our knowledge, etched-cavity LDs were not previously reported with GaSb-based LDs and our results thus establish a new building block for this technology.

In addition, our results show that GaSb buffer-layers grown by MOVPE on on-axis 300-mm Si wafers are suitable for MBE regrowth of semiconductor lasers. This shows the potential of the large-dimension GaSb-on-Si MOVPE templates for future optoelectronics developments.

6. Conclusion

We have studied 2.3-µm etched-cavity GaSb-based laser diodes (LDs) epitaxially integrated on on-axis (001)Si and benchmarked them against their cleaved facet counterparts. The LDs

Optics EXPRESS

were grown by MBE on a GaSb-on-Si template previously grown by MOVPE in a 300-mm reactor. Broad-area cleaved-cavity LDs exhibit a threshold current density around 660 A.cm^{-2} demonstrating that MOVPE GaSb-on-Si templates are a suitable platform for optoelectronic devices overgrowth. In addition, different etched-facet geometries operate in continuous wave well above room temperature, and their performance are similar to those of cleaved-cavity LDs. These results show that etching mirrors is a viable route to form laser cavities in the GaSb technology. Altogether this opens the way to the large-dimension epitaxial integration of mid-infrared semiconductor lasers with CMOS-compatible Si substrates and to PICs development.

Funding

H2020 LEIT Information and Communication Technologies (780240); Agence Nationale de la Recherche (ANR-10-IRT-05, ANR-11-EQPX-0016, ANR-15-IDEX-02, IRT NANOELEC).

Acknowledgments

T.B. acknowledges the French Renatech network. E.T. gratefully acknowledges the Japanese Society for the Promotion of Science (long-term fellowship #L-19509) and Prof. Y. Arakawa for his generous hospitality at U. Tokyo.

Disclosures

The authors declare no conflicts of interest.

References

1. I. E. Gordon, L. S. Rothman, C. Hill, R. V. Kochanov, Y. Tan, P. F. Bernath, M. Birk, V. Boudon, A. Campargue, K. V. Chance, B. J. Drouin, J.-M. Flaud, R. R. Gamache, J. T. Hodges, D. Jacquemart, V. I. Perevalov, A. Perrin, K. P. Shine, M.-A. H. Smith, J. Tennyson, G. C. Toon, H. Tran, V. G. Tyuterev, A. Barbe, A. G. Császár, V. M. Devi, T. Furtenbacher, J. J. Harrison, J.-M. Hartmann, A. Jolly, T. J. Johnson, T. Karman, I. Kleiner, A. A. Kyuberis, J. Loos, O. M. Lyulin, S. T. Massie, S. N. Mikhailenko, N. Moazzen-Ahmadi, H. S. P. Müller, O. V. Naumenko, A. V. Nikitin, O. L. Polyansky, M. Rey, M. Rotger, S. W. Sharpe, K. Sung, E. Starikova, S. A. Tashkun, J. V. Auwera, G. Wagner, J. Wilzewski, P. Wcisło, S. Yu, and E. J. Zak, "The HITRAN2016 molecular spectroscopic database," J. Quant. Spectrosc. Radiat. Transfer **203**, 3–69 (2017).
2. G. Belenky, L. Shterengas, M. V. Kisin, and T. Hosoda, "Gallium antimonide (GaSb)-based type-I quantum well diode lasers: recent development and prospects," in *Semiconductor Lasers* (Elsevier, 2013), pp. 441–486.
3. L. Cerutti, A. Vicet, and E. Tournié, "Interband mid-infrared lasers," in *Mid-Infrared Optoelectronics* (Elsevier, 2020), pp. 91–130.
4. R. Wang, A. Vasiliev, M. Muneeb, A. Malik, S. Sprengel, G. Boehm, M.-C. Amann, I. Šimonytė, A. Vizbaras, K. Vizbaras, R. Baets, and G. Roelkens, "III–V-on-Silicon Photonic Integrated Circuits for Spectroscopic Sensing in the 2–4 μm Wavelength Range," Sensors **17**(8), 1788 (2017).
5. A. Y. Liu and J. Bowers, "Photonic Integration With Epitaxial III–V on Silicon," IEEE J. Sel. Top. Quantum Electron. **24**(6), 1–12 (2018).
6. B. Schwarz, P. Reininger, D. Ristanić, H. Detz, A. M. Andrews, W. Schrenk, and G. Strasser, "Monolithically integrated mid-infrared lab-on-a-chip using plasmonics and quantum cascade structures," Nat. Commun. **5**(1), 4085 (2014).
7. M. Hitaka, T. Dougakiuchi, A. Ito, K. Fujita, and T. Edamura, "Stacked quantum cascade laser and detector structure for a monolithic mid-infrared sensing device," Appl. Phys. Lett. **115**(16), 161102 (2019).
8. M. Rio Calvo, L. Monge-Bartolome, M. Bahriz, G. Boissier, L. Cerutti, J.-B. Rodriguez, and E. Tournié, "Mid-infrared laser diodes epitaxially grown on on-axis (001) silicon," Optica **7**(4), 263–266 (2020).
9. T. Cerba, M. Martin, J. Moeyaert, S. David, J. L. Rouviere, L. Cerutti, R. Alcotte, J. B. Rodriguez, M. Bawedin, H. Boutry, F. Bassani, Y. Bogumilowicz, P. Gergaud, E. Tournié, and T. Baron, "Anti phase boundary free GaSb layer grown on 300 mm (001)-Si substrate by metal organic chemical vapor deposition," Thin Solid Films **645**, 5–9 (2018).
10. R. Yang, N. Su, P. Bonfanti, J. Nie, J. Ning, and T. T. Li, "Advanced in situ pre-Ni silicide (Siconi) cleaning at 65 nm to resolve defects in NiSix modules," J. Vac. Sci. Technol., B: Nanotechnol. Microelectron.: Mater., Process., Meas., Phenom. **28**(1), 56–61 (2010).
11. M. Martin, D. Caliste, R. Cipro, R. Alcotte, J. Moeyaert, S. David, F. Bassani, T. Cerba, Y. Bogumilowicz, E. Sanchez, Z. Ye, X. Y. Bao, J. B. Pin, T. Baron, and P. Pochet, "Toward the III–V/Si co-integration by controlling the biatomic steps on hydrogenated Si(001)," Appl. Phys. Lett. **109**(25), 253103 (2016).
12. H. Kroemer, "Polar-on-nonpolar epitaxy," J. Cryst. Growth **81**(1-4), 193–204 (1987).

Optics EXPRESS

13. E. Tournié, "Molecular-Beam Epitaxy of Antimonides for Optoelectronic Devices," in *Molecular Beam Epitaxy* (John Wiley & Sons Ltd, 2019), pp. 233–246.
14. J. R. Reboul, L. Cerutti, J. B. Rodriguez, P. Grech, and E. Tournié, "Continuous-wave operation above room temperature of GaSb-based laser diodes grown on Si," Appl. Phys. Lett. **99**(12), 121113 (2011).
15. A. Castellano, L. Cerutti, J. B. Rodriguez, G. Narcy, A. Garreau, F. Lelarge, and E. Tournié, "Room-temperature continuous-wave operation in the telecom wavelength range of GaSb-based lasers monolithically grown on Si," APL Photonics **2**(6), 061301 (2017).
16. L. Coldren, K. Furuya, B. Miller, and J. Rentschler, "Etched mirror and groove-coupled GaInAsP/InP laser devices for integrated optics," IEEE J. Quantum Electron. **18**(10), 1679–1688 (1982).
17. J. Yang, Z. Mi, and P. Bhattacharya, "Groove-Coupled InGaAs/GaAs Quantum Dot Laser/Waveguide on Silicon," J. Lightwave Technol. **25**(7), 1826–1831 (2007).